Gd and Eu Co-Doped Nanoscale Metal–Organic Framework as a T_1–T_2 Dual-Modal Contrast Agent for Magnetic Resonance Imaging

Geoffrey D. Wang[1], Hongmin Chen[1,2], Wei Tang[1], Daye Lee[1], and Jin Xie[1,2]

[1]Department of Chemistry, University of Georgia, Athens, Georgia; and [2]Bio-Imaging Research Center, University of Georgia, Athens, Georgia

Corresponding Authors:
Hongmin Chen,
Department of Chemistry and the Bio-Imaging Research Center,
University of Georgia, Athens, GA 30602,
E-mail: hchen@uga.edu; and Jin Xie,
E-mail: jinxie@uga.edu

Key Words: dual modal, fluorescence, MRI, dual mode, contrast agent, gadolinium, MOF

Abbreviations: Nanoscale metal–organic framework (NMOF), magnetic resonance imaging (MRI), europium (Eu), gadolinium (Gd), isophthalic acid (H_2IPA), polyvinylpyrrolidone (PVP), hexamethylenetetramine (HMTA), dimethyl formamide (DMF), tetraethylorthosilicate (TEOS), (3-aminopropyl) triethoxysilane (APTES), Fourier transform infrared (FT-IR), phosphate-buffered saline (PBS), magnetic resonance (MR), fast-spin echo (FSE), repetition time (TR), field-of-view (FOV), spin-echo multi sections (SEMS), fast spin-echo multi-section sequence (FSEMS), arginylglycylaspartic acid (RGD), 3-(4,5-dimethylthiazol-2-yl)-2,5-diphenyltetrazolium bromide (MTT)

ABSTRACT

Recently, a growing interest has been seen in the development of T_1–T_2 dual-mode probes that can simultaneously enhance contrast on T_1- and T_2-weighted images. A common strategy is to integrate T_1 and T_2 components in a decoupled manner into a nanoscale particle. This approach, however, often requires a multi-step synthesis and delicate nanoengineering, which may potentially affect the production and wide application of the probes. We herein report the facile synthesis of a 50-nm nanoscale metal–organic framework (NMOF) comprising gadolinium (Gd^{3+}) and europium (Eu^{3+}) as metallic nodes. These nanoparticles can be prepared in large quantities and can be easily coated with a layer of silica. The yielded Eu,Gd-NMOF@SiO_2 nanoparticles are less toxic, highly fluorescent, and afford high longitudinal (38 $mM^{-1}s^{-1}$) and transversal (222 $mM^{-1}s^{-1}$) relaxivities on a 7 T magnet. The nanoparticles were conjugated with c(RGDyK), a tumor-targeting peptide sequence, which has a high binding affinity toward integrin $\alpha_v\beta_3$. Eu,Gd-NMOF@SiO_2 nanoparticles, when intratumorally or intravenously injected, induce simultaneous signal enhancement and signal attenuation on T_1-and T_2-weighted images, respectively. These results suggest great potential of the NMOFs as a novel T_1–T_2 dual-mode contrast agent.

INTRODUCTION

Magnetic resonance imaging (MRI) is one of the most widely used diagnostic tools in clinics. MRI affords a number of advantages such as noninvasiveness, high spatial and temporal resolutions, and good soft tissue contrast (1, 2). However, the intrinsic MRI signals are often suboptimal in delineating internal organs and diseased tissues. To improve imaging quality, contrast agents, often in the form of paramagnetic compounds or superparamagnetic nanoparticles, are administered before or during an MRI scan (3-5). These magnetic agents alter local magnetic environments, inducing shortened longitudinal relaxation times (T_1) and transverse relaxation times (T_2). Although most agents shorten both T_1 and T_2, the impact is often dominant on one side. So far in clinics, the most commonly used T_1 agents are gadolinium (Gd) complexes (6) and those for T_2 imaging are iron oxide nanoparticles (7).

Recently, a growing interest has been seen in the development of T_1–T_2 dual-mode contrast agents that can simultaneously modulate T_1- and T_2-weighted contrasts. Such a technology is attractive because MRI has an intrinsic high background signal. Even with conventional T_1 and T_2 contrast agents, the diagnosis can often be affected by artifacts caused by truncation, motion, aliasing, or chemical shift (8). T_1–T_2 dual-mode imaging may minimize the risks of ambiguity and improve image conspicuity and diagnostic sensitivity (9-11). To this end, there have been some efforts of integrating T_1 and T_2 contrast components using nanoscale engineering. These include tethering Gd-complex onto the surface of iron oxide nanoparticles (12), doping Gd cations into the matrix of iron oxide nanoparticles (13, 14), and forming a core/shell nanostructure where the T_1 and T_2 components are magnetically decoupled (15, 16). However, these approaches often involve a multi-step synthesis and/or a delicate control over the interaction between the T_1 and

ISSN 2379-1381 http://dx.doi.org/10.18383/j.tom.2016.00226

T_2 components, which may potentially limit their production and applications.

Herein, we report the facile synthesis of a novel, nanoscale metal–organic framework (NMOF)-based T_1–T_2 dual-modal contrast agent. In particular, using isophthalic acid (H_2IPA) as building blocks, Eu^{3+} and Gd^{3+} as metallic nodes, and polyvinylpyrrolidone (PVP) as a surfactant, as reaction precursors, we prepared ~50 nm of self-assembled Eu,Gd-NMOFs in large quantities. Unlike conventional NMOFs, which are rapidly degraded in an aqueous environment (17), our Eu,Gd-NMOFs are stable in water for up to 24 hours because of strong interactions between the lanthanides and H_2IPA as well as between the lanthanides and the PVP coating. To improve the particle stability against transmetallation, the Eu,Gd-NMOFs were further coated with a layer of silica. The resulting Eu,Gd-NMOFs@SiO_2 particles manifested both high r_1 and high r_2 relaxivities (38 $mM^{-1}s^{-1}$ and 222 $mM^{-1}s^{-1}$, respectively), suggesting their potential as a T_1–T_2 dual-modal contrast agent. Such a possibility was demonstrated first in vitro and then in vivo with either intratumorally or intravenously injected nanoparticles, resulting in simultaneous hyperintensities and hypointensities on T_1-and T_2-weighted images, respectively. Meanwhile, Eu,Gd-NMOF@SiO_2 nanoparticles also afford strong fluorescence that permits in vitro and potentially histological analysis of nanoparticle location within tissue specimens. Overall, the Eu,Gd-NMOFs can be synthesized in a straightforward and high-throughput fashion and afford excellent magnetic and optical properties, suggesting their great potential as a novel and versatile multimodal imaging probe.

METHODOLOGY

Materials

The following materials have been used in this study: $Gd(NO_3)_3{\cdot}6H_2O$, $Eu(NO_3)_3{\cdot}6H_2O$, H_2IPA, PVP40, hexamethylenetetramine (HMTA), dimethylformamide (DMF), tetrahydrofuran, tetraethylorthosilicate (TEOS), (3-aminopropyl) triethoxysilane (APTES), ammonia, and ethanol. All these materials were purchased from Aldrich (Sigma-Aldrich, St. Louis, Missouri) and used without further purification.

Synthesis of Eu,Gd-NMOF

In a typical synthesis, H_2IPA (1 mg), $Gd(NO_3)_3{\cdot}6H_2O$ (10 mg), $Eu(NO_3)_3{\cdot}6H_2O$ (0.5 mg), PVP (60 mg), and HMTA (16 mg) were first dissolved in a mixed solution containing 1.0 mL of DMF and 4.0 mL of water. Precursors of other ratios were also tested. The mixture was heated at 100°C for 4 minutes to induce Eu,Gd-NMOF growth. The resulting Eu,Gd-NMOFs were collected by centrifugation, washed with ethanol, and resuspended in ethanol for further characterization. For comparison, the synthesis was also performed without HMTA or H_2IPA.

Synthesis of Silica-Coated Eu,Gd-NMOF (Eu,Gd-NMOF@SiO_2)

Eu,Gd-NMOF@SiO_2 was prepared by mixing 10 mg of the as-synthesized Eu,Gd-NMOF with 100 μL of TEOS, 10 μL of APTES, and 0.5 mL of ammonia (28%) in 15 mL of ethanol at room temperature overnight. The Eu,Gd-NMOF@SiO_2 was isolated by centrifugation at 10 000 rpm for 10 minutes.

Bio-Conjugation (Preparation of Arginylglycylaspartic Acid [RGD]-NMOF@SiO_2)

For bio-conjugation, 50 mg of Eu,Gd-NMOF@SiO_2 nanoparticles were dispersed in a borate buffer (50 mM, pH 8.3) with magnetic stirring. Into this solution, 0.5 mg of bis(sulfosuccinimidyl)suberate was added in 0.1 mL of dimethyl sulfoxide. After 0.5 hours, the conjugate intermediate was collected by centrifugation and redispersed in the borate buffer (50 mM, pH 8.3). c(RGDyK) in dimethyl sulfoxide was added to the solution, and the mixture was incubated at room temperature for 2 hours to form RGD-Eu,Gd-NMOF@SiO_2 nanoparticles.

Characterizations

All transmission electron microscopy images were obtained on an FEI Tecnai 20 transmission electron microscope operating at 200 kV (FEI, Hillsboro, Oregon). Optical measurements were performed at room temperature under ambient air conditions. Ultraviolet-visible absorption spectra were recorded on a Shimdzu 2450 UV-Vis spectrometer (Shimadzu Scientific, Columbia, Maryland). Fluorescence measurements were performed using a Hitachi F-7000 spectrofluorimeter (Hitachi America, Tarrytown, New York). Fourier transform infrared (FT-IR) spectra were recorded on a Nicolet iS10 FT-IR Spectrometer (Thermo Scientific, Waltham, Massachusetts). Powder X-ray diffraction intensity data were collected on a PANalytical X'Pert PRO MRD powder diffractometer using Cu Kα radiation (ASD Inc., Boulder, Colorado).

Stability of Eu,Gd-NMOF and Eu,Gd-NMOF@SiO_2 in Water and Phosphate-Buffered Saline

Here, 5 mg of Eu,Gd-NMOFs or Eu,Gd-NMOF@SiO_2 were dispersed in 1 mL of aqueous solutions, with pH ranging from 3 to 11. Gentle agitation was applied. After 24 hours, aliquots of the solution were taken to measure the change in fluorescent intensity.

MRI Phantom Study

Eu,Gd-NMOF@SiO_2 with Gd concentrations ranging from 5×10^{-5} to 0.08 mM were suspended in 1% agarose gel in 300 μL polymerase chain reaction tube. These tubes were then embedded in a homemade tank designed to fit the MRI coil. T_1- and T_2-weighted magnetic resonance (MR) images of the samples were acquired on a 7 T small animal MRI system (Varian Medical Systems, Inc., Palo Alto, California). For T_1-weighted images, a T_1 inversion recovery fast-spin echo (FSE) sequence was used with the following parameters: repetition time (TR) = 5000 milliseconds, echo time (TE) = 12 milliseconds, echo train length = 8, inversion times = 5, 10, 30, 50, 80, 200, 500, 700, 900, 1200, and 3000 milliseconds. For T_2-weighted images, an FSE sequence was used with the following parameters: TR = 3000 milliseconds, TE = 10–100 milliseconds, with the step size set at 10 milliseconds. For both imaging sets, the following section settings were applied: field-of-view (FOV) = 65 × 65 mm^2; matrix size = 256 × 256; coronal sections = 4 with section thickness = 1 mm.

Cell Culture

U87MG (human glioblastoma) cells (ATCC) were grown in Dulbecco's Modified Eagle Medium supplemented with 10% fetal

bovine serum and 100 U/mL of penicillin/streptomycin (ATCC). The cells were maintained in a humidified incubator with 5% carbon dioxide (CO_2) atmosphere at 37°C.

Toxicity of NMOF In Vitro

U87MG cells were seeded into a 96-well culture plate at a density of 10 000 cells/well and were cultured overnight. The media were removed and replaced with fresh media containing different Eu,Gd-NMOF@SiO_2 concentrations (0–50 μM Gd^{3+}). Plates were incubated for 24 hours at 37°C and 5% CO_2. Viability was measured by 3-(4,5-dimethylthiazol-2-yl)-2,5-diphenyltetrazolium bromide (MTT) assays (18).

Cell Uptake

U87MG cells were incubated with Eu,Gd-NMOF@SiO_2 or RGD-Eu,Gd-NMOF@SiO_2 (20 μg/mL) in a chamber slide for 1 hour. U87MG cells only served as a negative control. After the incubation, the cells were washed 3 times with phosphate-buffered saline (PBS) to remove unbound nanoparticles. The slides were then imaged on an Olympus (Olympus Co. of U.S.A., Center Valley, Pennsylvania) X71 fluorescence microscope.

In Vitro MRI with Cell Pellets

U87MG cells were cultured until ~70% confluency was reached. Cells were then washed with PBS, and incubated with 2 mL of media containing 100 μg of RGD-Eu,Gd-NMOF@SiO_2 or Eu,Gd-NMOF@SiO_2. After 1 hour, the media were removed and cells were collected as pellets in 200 μL tubes. These tubes were then embedded in a homemade tank designed to fit the MRI coil. T_1- and T_2-weighted MR images were acquired on a 7 T small animal MRI system (Varian) using an FSE sequence with the following parameters: TR/TE = 500/14 milliseconds (T_1), TR/TE = 3000/8 milliseconds (T_2), section thickness = 0.5 mm, FOV = 60 × 50 mm, echo train length = 8, matrices = 256 × 256, and repeated three times.

In Vivo MRI with Subcutaneously Injected Nanoparticles

Animal studies were performed according to a protocol approved by the Institutional Animal Care and Use Committee (IACUC) of the University of Georgia. Before the in vivo experiments, the Eu,Gd-NMOF@SiO_2 nanospheres were filtered through sterilized membrane filters (pore size = 0.22 μm) and stored in sterilized vials. U87MG cancer cells were subcutaneously inoculated into the right flanks of a 6-week-old nude

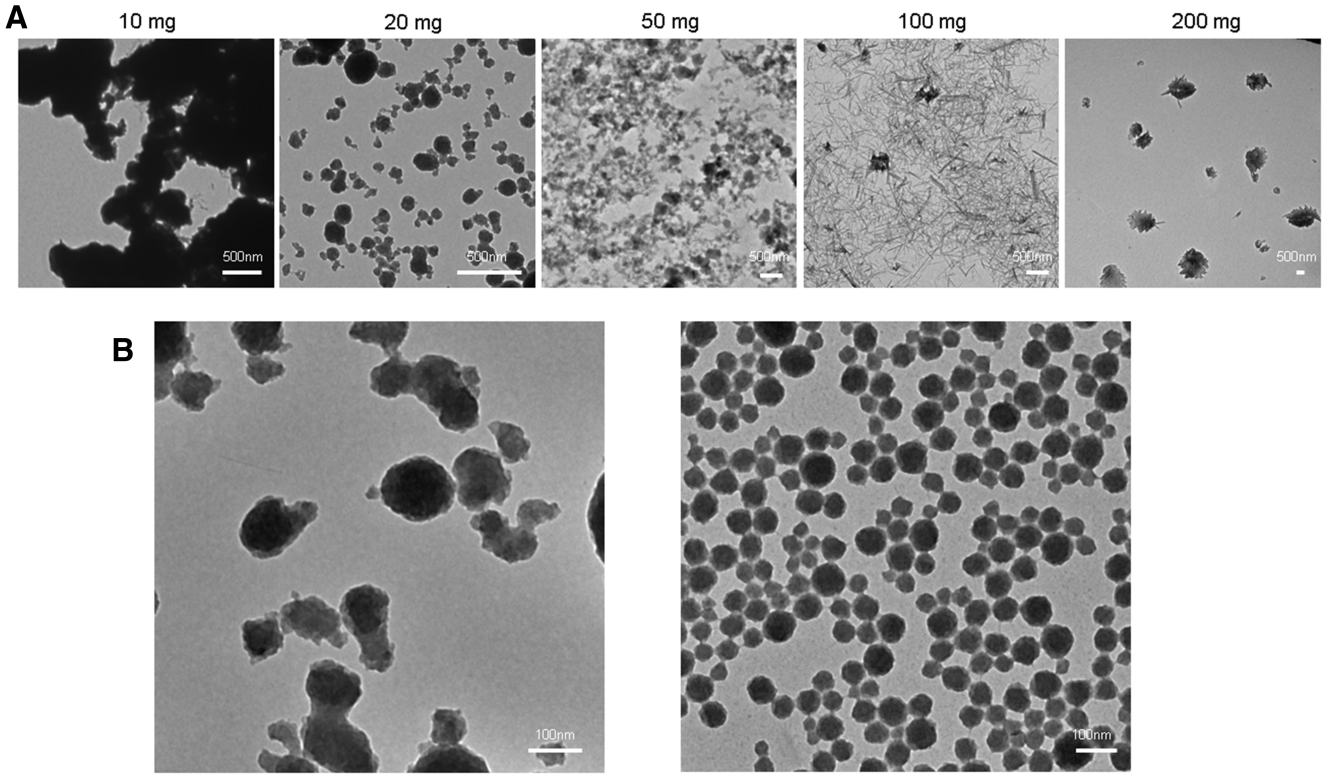

Figure 1. Synthesis of Eu,Gd-NMOFs. Poor size control if hexamethylenetetramine (HMTA) and polyvinylpyrrolidone (PVP) are not used as reactants (A). Despite the ratio between the lanthanide cations and isophthalic acid (H_2IPA) (the amount of which increased from 10 to 200 mg), the nanoparticle products showed poor size distribution. Notably, the synthesis was conducted in a dimethylformamide (DMF)/tetrahydrofuran (THF) solvent, as the resulting nanoscale metal–organic frameworks (NMOFs) were not stable in water. The impact of HMTA and PVP on the nanoparticle formation (B). Left, when HMTA was added to the precursors, Eu,Gd-NMOFs were formed in a DMF/water solvent, but the particle showed a wide size distribution. Right, when both HMTA and PVP were used, uniform Eu,Gd-NMOFs were obtained.

mice. Imaging was performed ~3 weeks later on a 7 T small animal MRI system (Varian). T_1- and T_2-weighted MR images were acquired using spin-echo multi sections sequence (SEMSs) and fast spin-echo multi-section sequence (FSEMS), respectively, with the following parameters: TR/TE = 500/14 milliseconds (T_1) and TR/TE = 3000/33 milliseconds (T_2), section thickness = 1.0 mm, FOV = 60 × 50 mm, matrices = 256 × 256, and repeated three times. Further, 0.8 mg/kg of Eu,Gd-NMOF nanospheres were intratumorally injected. T_1- and T_2-weighted MR images before and 4 hours after the injection were acquired.

In Vivo Liver MRI with Systemically Injected Nanoparticles.

Six-week-old female BALB/c mice were imaged on a 7 T small animal MRI system (Varian). T_1- and T_2-weighted MR images were acquired using SEMSs and FSEMS with the following parameters: TR/TE = 500/16 milliseconds (T_1) and TR/TE = 2500/8.65 milliseconds (T_2), section thickness = 1.0 mm, FOV = 30 × 30 mm, and matrices = 256 × 256. Further, 0.8 mg/kg of Eu,Gd-NMOFs were intravenously injected. T_1- and T_2-weighted MR images of the liver before and 4 hours after the injection were acquired.

RESULTS AND DISCUSSION

Synthesis and Characterization of Eu,Gd-NMOFs

Eu,Gd-NMOFs were synthesized by mixing H_2IPA, $Gd(NO_3)_3$, $Eu(NO_3)_3$, HMTA and PVP in a mixed solution containing DMF and water, and the solution was heating at 100°C. Previously, Oh et al. reported NMOF synthesis with Gd^{3+}, Eu^{3+}, and H_2IPA in a mixed solvent containing polar aprotic DMF and tetrahydrofuran (19). However, the method has poor size controls over the NMOF products. As manifested in Figure 1A, when using different amounts of H_2IPA, Eu,Gd-NMOFs of varied morphologies were obtained, but all the products showed a wide size distribution (Figure 1A). Moreover, Eu,Gd-NMOFs synthesized using this method were immediately degraded in water (data not

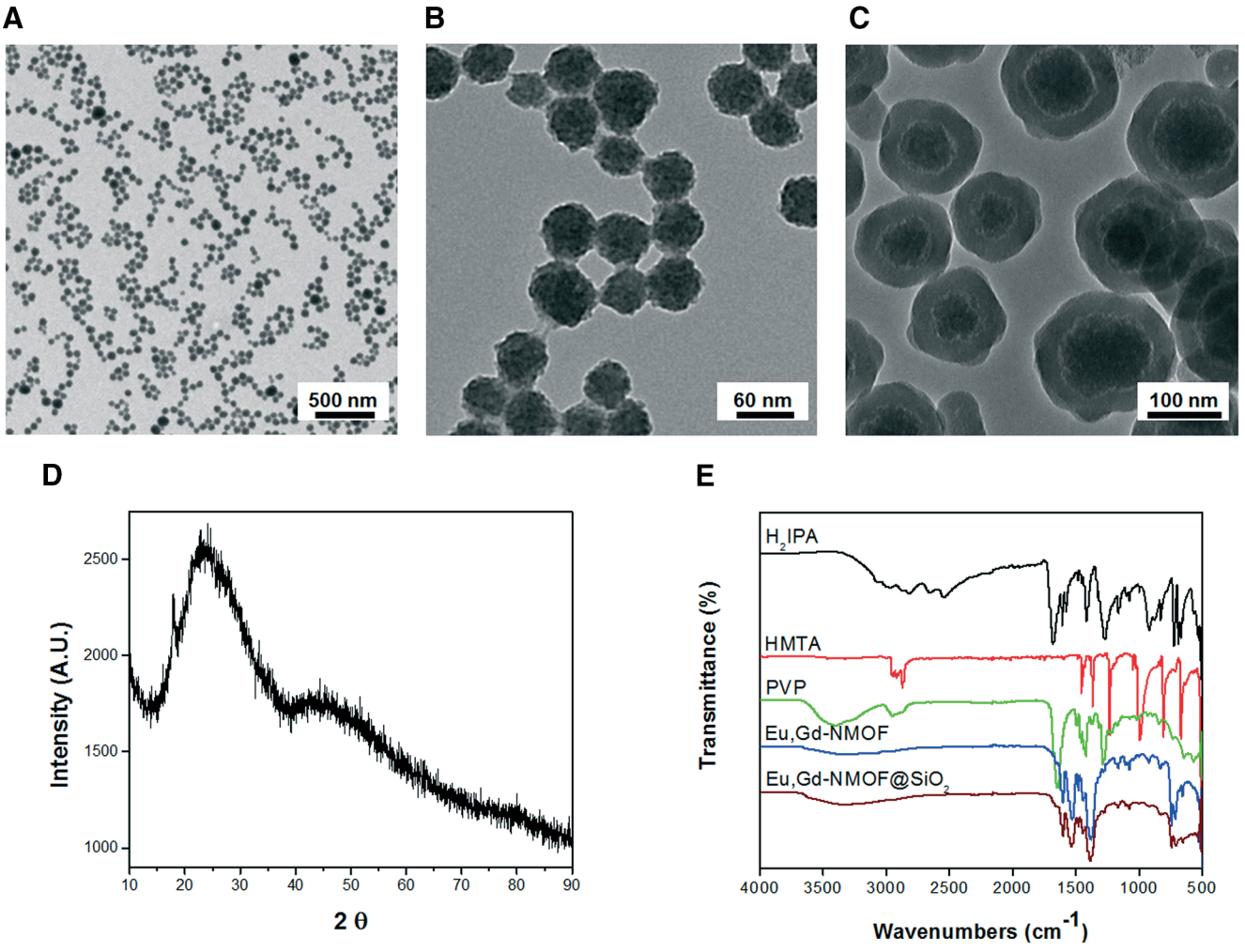

Figure 2. Characterization of Eu,Gd-NMOF@SiO_2. Transmission electron microscopy (TEM) images of as-synthesized Eu,Gd-NMOF nanospheres on a large scale (A, B). TEM image of the core-shell structure of Eu,Gd-NMOF@SiO_2 (protection SiO_2 layer ~30 nm) (C). X-ray diffraction (XRD) pattern of Eu,Gd-NMOF@SiO_2 nanospheres (D). Fourier transform infrared (FT-IR) spectra of H_2IPA, HMTA, PVP, Eu,Gd-NMOFs, and Eu,Gd-NMOF@SiO_2 nanospheres (E).

shown), which is a potential problem for bioapplications. To address the issue, we added HMTA to the reaction solution. HMTA increased the pH of the initial reaction solution from ~5.0 to ~8.15, and as such, promoted the ionization and coordination of H_2IPA with Gd^{3+} and Eu^{3+} (20). Furthermore, we also included PVP as part of the precursors, which was bound to the growing nanoparticle surface to improve the particle stability and control their growth. By adding HMTA and PVP to the reactants, Eu,Gd-NMOFs of narrow size distribution were obtained in a DMF/water mixed solvent (Figure 1B). As a comparison, without the 2 agents, no NMOF was formed under the same condition (data not shown).

Transmission emission microscopy shows that the resulting Eu,Gd-NMOFs were spherical and had an average size of 50 ± 12 nm (Figure 2, A and B). The Eu,Gd-NMOFs were very stable in aqueous solutions, which is rare among NMOFs (17). However, the particles still decomposed when the aqueous solution had a relatively high ionic strength, for instance, PBS. This is presumably due to transmetallation and lanthanides binding with PO_4^{3-}. To further improve the particle stability, a silica coating was imparted to the surface of Eu,Gd-NMOFs. In particular, we followed the Stöber method (21, 22) and used both TEOS and APTES as silane precursors in the coating. The resulting Eu,Gd-NMOF@SiO_2 particles have a coating thickness of ~30 nm and an overall diameter of 100 ± 20 nm (Figure 2C). X-ray diffraction analysis found a broad peak at around 22.5° (2θ) (Figure 2D), which corresponds to the diffraction by Eu,Gd-NMOFs (JCPDS No. 01-086-1561). Similar results were observed by others in previous studies (23). FT-IR found absorption bands at 1609 cm^{-1} and 1558 cm^{-1} for Eu,Gd-NMOF and Eu,Gd-NMOF@SiO_2 respectively (Figure 2E). These absorption bands correspond to the C=O stretch, confirming successful H_2IPA coordination in the system. For the as-synthesized Eu,Gd-NMOFs, there was broad absorption band at around 3600 cm^{-1}, suggesting residual PVP coating on the nanoparticles (Figure 2E). Meanwhile, no characteristic HMTA absorption band at 1370 cm^{-1} (attributed to the C-N stretch) was observed with

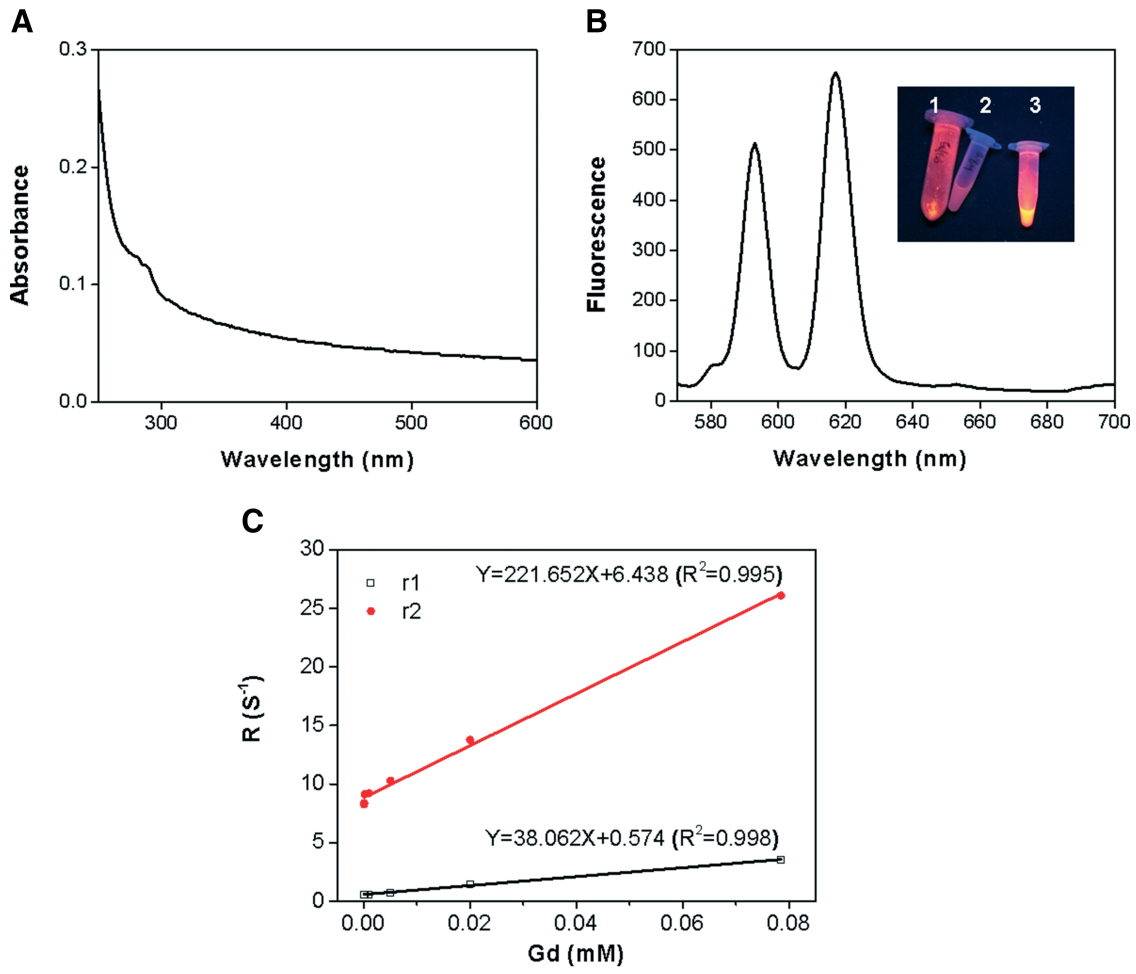

Figure 3. Optical and magnetic properties of Eu,Gd-NMOF@SiO_2. Ultraviolet-visible absorbance of Eu,Gd-NMOF@SiO_2 nanospheres (A). Fluorescent spectrum of Eu,Gd-NMOF@SiO_2. The inset is a photograph of (1) Eu,Gd-NMOF@SiO_2 powder, (2) water, and (3) aqueous solution of Eu,Gd-NMOF@SiO_2 (B). Relaxivity measurements of Eu,Gd-NMOF@SiO_2. Changes in R_1 ($1/T_1$) and R_2 ($1/T_2$) were plotted over various Gd concentration. r_1 and r_2 relaxivities were 38 $mM^{-1}s^{-1}$ and 222 $mM^{-1}s^{-1}$, respectively (C).

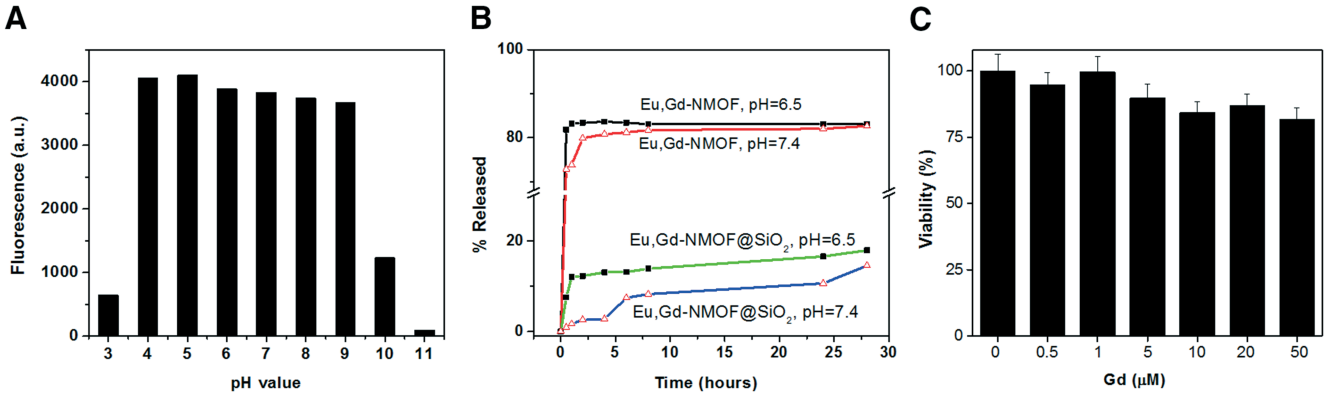

Figure 4. Stability and cytotoxicity. Fluorescence intensity (ex/em: 360/595 nm) changes when Eu,Gd-NMOF@SiO_2 nanospheres are incubated in aqueous solutions of different pH (A). Gd^{3+} release profiles of Eu,Gd-NMOFs and Eu,Gd-NMOF@SiO_2 nanospheres in phosphate-buffered saline (PBS) (pH = 6.5 and 7.4) (B). Cell viability is assessed by 3-(4,5-dimethylthiazol-2-yl)-2,5-diphenyltetrazolium bromide (MTT) assays with U87MG cells. Eu,Gd-NMOF@SiO_2 nanospheres with a Gd concentration ranging from 0 to 50 μM were incubated with cells (C).

Eu,Gd-NMOF, suggesting minimal adsorption of HMTA on the particle surface (Figure 2E).

Optical and Magnetic Properties of Eu,Gd-NMOF@SiO_2

Eu,Gd-NMOF@SiO_2 nanoparticles absorb at around 280 nm (Figure 3A) and have strong emission at 594 and 620 nm (Figure 3B). These 2 emission peaks are attributed to $^5D_0 \rightarrow {}^7F_1$ and $^5D_0 \rightarrow {}^7F_2$ transitions, respectively (24-26). Such fluorescence can be used to track the nanoparticles in vitro and in histological studies.

The MRI contrast ability of the Eu,Gd-NMOF@SiO_2 nanoparticles was evaluated by phantom studies on a 7 T magnet. In brief, Eu,Gd-NMOF@SiO_2 nanoparticles of increased concentrations were dispersed in 1% agarose gel, and the samples were scanned by MRI using SEMSs and FSEMSs. For both T_1- and T_2-weighted imaging, the signals were clearly concentration-dependent. In particular, significant signal enhancement was observed in T_1 images at elevated concentrations; in contrast, in T_2 images, signal reduction was observed at high particle concentrations. On the basis of the imaging results, it was deduced that r_1 was 38 $mM^{-1}s^{-1}$ and r_2 was 222 $mM^{-1}s^{-1}$ (Figure 3C). These relaxivity values are much higher than commonly used clinical contrast agents such as Gd–diethylenetriamine pentaacetic acid (r_1 of 3.10 $mM^{-1}s^{-1}$) and Feridex (r_2 of 117 $mM^{-1}s^{-1}$) (27). The exact mechanisms behind the high r_1 and r_2 values are unclear, but it may be attributed to the rigid confinement of Gd^{3+} in the nanosystem and slow interex-

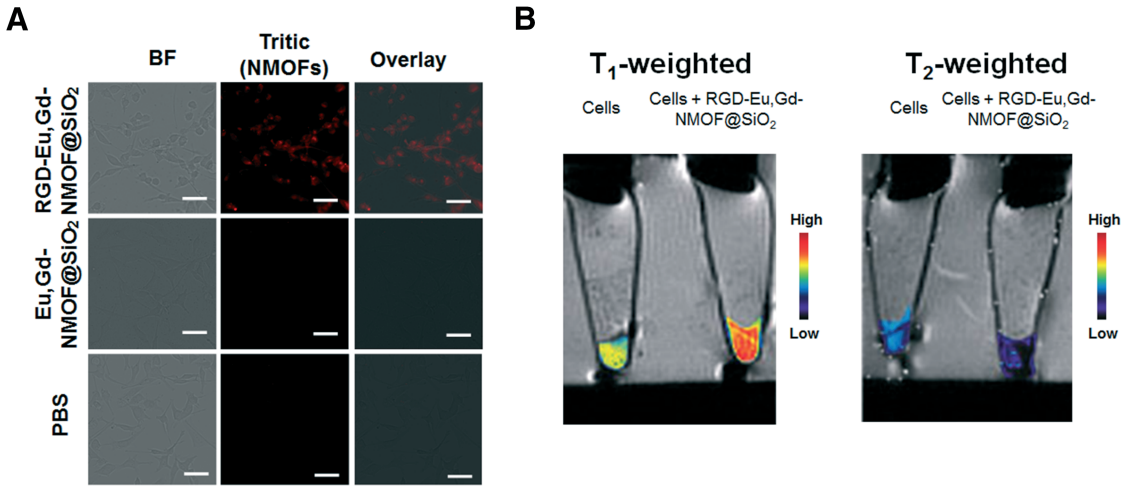

Figure 5. Cell fluorescence microscopy and magnetic resonance imaging (MRI). Fluorescent images of U87MG cells that had been incubated for 1 hour with Eu,Gd-NMOF@SiO_2 or RGD-Eu,Gd-NMOF@SiO_2. Scale bars: 50 μm (A). T_1- and T_2-weighted MRI of cells that had, or had not, been incubated with RGD-Eu,Gd-NMOF@SiO_2 (B).

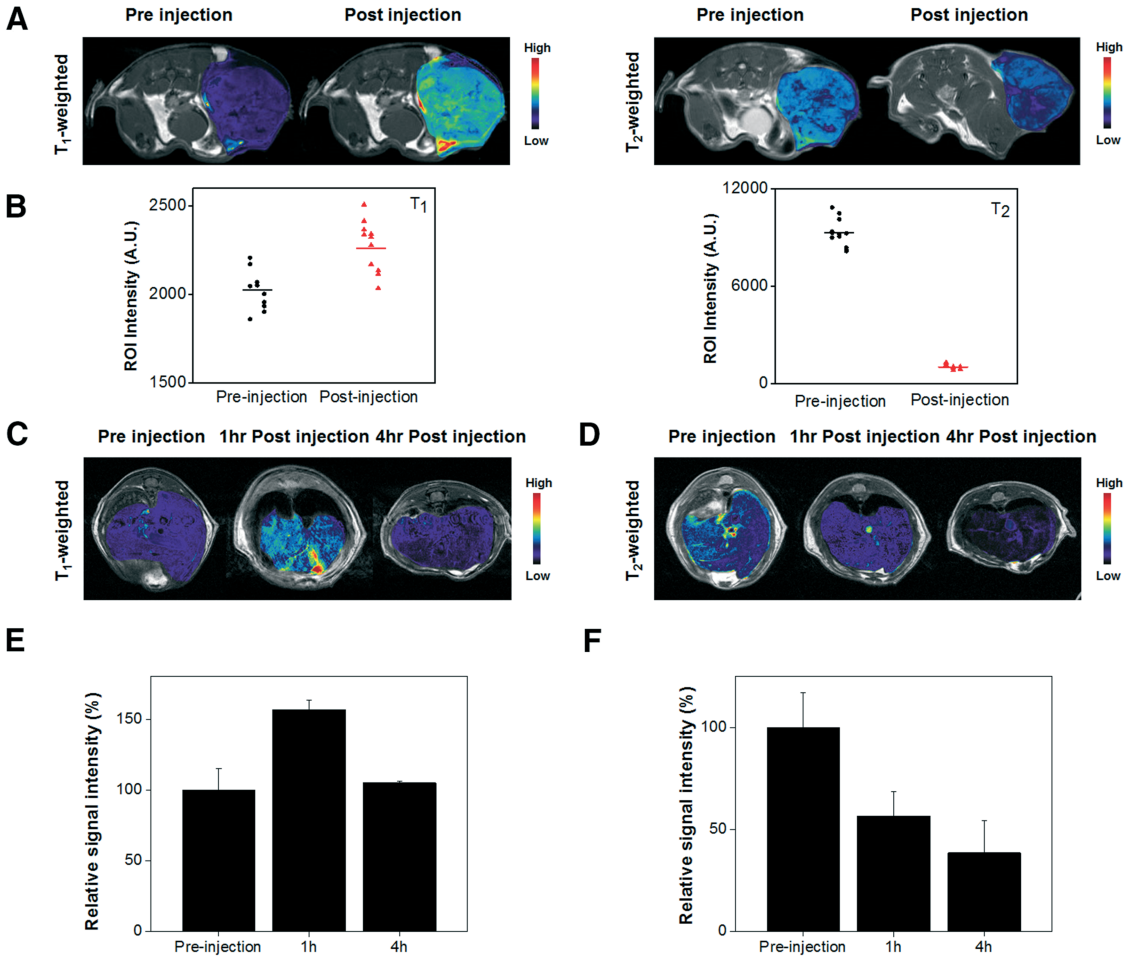

Figure 6. In vivo MRI studies. Axial T_1- and T_2-weighted images, taken before and after intratumoral injection of Eu,Gd-NMOF@SiO_2 nanospheres (A). Signal change before and after Eu,Gd-NMOF@SiO_2 nanosphere injection, based on the region-of-interest (ROI) analysis on multiple slides from (A) (B). Axial T_1-weighted images of the liver, acquired before and after intravenous injection of Eu,Gd-NMOF@SiO_2 nanospheres (C). Axial T_2-weighted images of the liver, acquired before and after intravenous injection of Eu,Gd-NMOF@SiO_2 nanospheres (D). Change of signals in the liver, based on ROI analysis on imaging results from (C) and (D), respectively (E, F).

change of Gd^{3+} with water molecules (28). The r_2/r_1 ratio is 5.8, which is at the boundary between conventionally defined T_1 and T_2 agents (29).

Nanoparticle Stability

The stability of Eu,Gd-NMOF@SiO_2 nanoparticles was studied by monitoring fluorescence changes in different solutions. These included aqueous solutions, with pH ranging from 3 to 11, and PBS. It was observed that the Eu,Gd-NMOF nanoparticles were very stable when the pH was maintained between 4 and 9, and only degraded when the pH was above 9 or below 4 (Figure 4A), suggesting great resistance of the particles against pH changes. In contrast, Eu,Gd-NMOFs were much more labile in PBS, and were largely dissolved within 1 hour (Figure 4B). With the silica coating, however, Eu,Gd-NMOF@SiO_2 showed significantly enhanced stability, showing no fluorescence drop in PBS for at least 28 hours (Figure 4B).

Cytotoxicity and Cell Uptake Studies

Cytotoxicity of the nanoparticles was evaluated by 3-(4,5-dimethylthiazol-2-yl)-2,5-diphenyltetrazolium bromide (MTT) assays with U87MG cells, a human glioblastoma cell line. We found no detectable cytotoxicity with Eu,Gd-NMOF@SiO_2 nanoparticles even at very high concentration investigated (20 μM Gd^{3+}), indicating good biocompatibility (Figure 4C).

Next, we investigated whether Eu,Gd-NMOF@SiO_2 can be visualized by MRI when internalized by cells. To investigate, we conjugated c(RGDyK), a cyclic peptide with high binding affinity against integrin $\alpha_v\beta_3$ (30), to the surface of Eu,Gd-NMOF@SiO_2. This was achieved by covalently linking the primary amine of c(RGDyK) and the amine groups on Eu,Gd-NMOF@SiO_2 surface using bis(sulfosuccinimidyl)suberate as a homo-dimer crosslinker. U87MG cells were then incubated with RGD-Eu,Gd-NMOF@SiO_2 andEu,Gd-NMOF@SiO_2 nanoparticles for 1 hour. Notably, U87MG cells are high in integrin $\alpha_v\beta_3$ expression (31).

Under a fluorescence microscope, we observed a significant increase in intracellular red fluorescence, suggesting efficient internalization of RGD-Eu,Gd-NMOF@SiO_2 (Figure 5A). As a comparison, Eu,Gd-NMOF@SiO_2 nanoparticles showed low cell uptake, indicating that the uptake was mainly mediated by RGD–integrin interaction.

Such RGD-Eu,Gd-NMOF@SiO_2-treated cells were also collected as cell pellets and scanned by MRI. On T_1-weighted images, significant signal enhancement was observed with cells that had been incubated with nanoparticles compared with those that had been not been incubated (Figure 5B). This is attributed to hyperintensities induced by RGD-Eu,Gd-NMOF@SiO_2 nanoparticles. Meanwhile, significant signal reduction was observed on T_2-weighted images (Figure 5B), which was attributed to hypointensities induced by the RGD-Eu,Gd-NMOF@SiO_2. These results confirm that Eu,Gd-NMOF@SiO_2-labeled cells can be visualized by both T_1- and T_2-weighted MRI and also by fluorescence microscopy.

In Vivo MRI

For a proof of concept, we investigated the dual-mode contrast capacity of Eu,Gd-NMOF@SiO_2 in two in vivo studies. In the first study, we intratumorally injected Eu,Gd-NMOF@SiO_2 (0.8 mg/kg in 100 μL PBS, n = 3) to U87MG models and scanned the animals on a 7 T magnet. Similar to the in vitro studies, relative to the prescans, there was significant signal enhancement on T_1-weighted images and signal reduction on T_2-weighted images (Figure 6, A and B). In particular, the average signals in tumors increased by 12% ± 6% on T_1-weighted images after injection and decreased by 89% ± 2% on T_2-weighted images. In the second study, Eu,Gd-NMOF@SiO_2 nanoparticles were intravenously injected (0.8 mg/kg) into BALB/c mice, and T_1- and T_2-weighted images of the liver area were acquired both before and 1 hour and 4 hours after the injections (Figure 6, C and D). It is well known that nanoparticles after systemic injection are efficiently accumulated in the liver, such as through uptake by Kupffer cells (32). Region of interest analysis showed that relative to the prescans, signals in the liver increased to 157% ± 9% on T_1-weighted images at 1 hour. Interestingly, the signal decreased to 105% ± 2% at 4 hours (relative to the prescans; Figure 6E). This is probably attributed to considerably high concentration of Eu,Gd-NMOF@SiO_2 in the liver at the time point, leading to signal saturation. Similar phenomenon has been observed by others (33, 34). Meanwhile, on T_2-weighted images, signals in the liver decreased to 57% ± 12% on T_2 images at 1 hour and to 38% ± 16% at 4 hours (Figure 6F). Overall, these results confirm the feasibility of using Eu,Gd-NMOF@SiO_2 nanoparticles as a T_1–T_2 dual-mode imaging probe.

CONCLUSIONS

We have developed a novel and facile procedure of synthesizing a highly hydrostable metal–organic framework, Eu,Gd-NMOFs. Silica-coated Eu,Gd-NMOFs exhibit high longitudinal (38 $mM^{-1}s^{-1}$) and transversal (222 $mM^{-1}s^{-1}$) relaxivities and strong fluorescence. In vitro and in vivo MRI studies confirm that Eu,Gd-NMOFs can induce both hyperintensities on T_1-weighted images and hypointensities on T_2-weighted images, suggesting great potential of the probe as a novel T_1–T_2 dual-mode imaging probe. The nanoparticle surface can be easily coupled with a variety of targeting moieties for different imaging purposes. It is also possible to impart onto the solid silica layer a mesoporous silica layer into which drug molecules can be loaded. These make the nanoparticles a modifiable platform technology that can find wide applications in modern imaging and theranostics.

ACKNOWLEDGMENTS

This research was supported by a DoD CDMRP grant (CA140666, J.X.), an NSF CAREER grant (NSF1552617, J.X.), and a UGA-GRU seed grant.

Conflict of Interest: None reported.

REFERENCES

1. Na HB, Song IC, Hyeon T. Inorganic nanoparticles for MRI contrast agents. Adv Mater. 2009;21(21):2133–2148.
2. Chen H, Zhen ZP, Todd T, Chu PK, Xie J. Nanoparticles for improving cancer diagnosis. Mater Sci Eng R Rep. 2013;74(3):35–69.
3. Chen H, Wang GD, Tang W, Todd T, Zhen ZP, Tsang C, Hekmatyar K, Cowger T, Hubbard RB, Zhang W, Stickney J, Shen B, Xie J. Gd-encapsulated carbonaceous dots with efficient renal clearance for magnetic resonance imaging. Adv Mater. 2014;26(39):6761–6766.
4. Yang H, Qin CY, Yu C, Lu Y, Zhang HW, Xue FF, Wu D, Zhou Z, Yang S. RGD-conjugated nanoscale coordination polymers for targeted T_1- and T_2-weighted magnetic resonance imaging of tumors in vivo. Adv Funct Mater. 2014;24(12):1738–1747.
5. Chen H, Wang GD, Sun XL, Todd T, Zhang F, Xie J, Shen B. Mesoporous silica as nanoreactors to prepare Gd-encapsulated carbon dots of controllable sizes and magnetic properties. Adv Funct Mater. 2016;26(22):3973–3982.
6. Caravan P. Strategies for increasing the sensitivity of gadolinium based MRI contrast agents. Chem Soc Rev. 2006;35(6):512–523.
7. Corot C, Robert P, Idee JM, Port M. Recent advances in iron oxide nanocrystal technology for medical imaging. Adv Drug Deliv Rev. 2006;58(14):1471–1504.
8. Krupa K, Bekiesińska-Figatowska M. Artifacts in magnetic resonance imaging. Pol J Radiol. 2015;80:93–106.
9. Kircher MF, de la Zerda A, Jokerst JV, Zavaleta CL, Kempen PJ, Mittra E, Pitter K, Huang R, Campos C, Habte F, Sinclair R, Brennan CW, Mellinghoff IK, Holland EC, Gambhir SS. A brain tumor molecular imaging strategy using a new triple-modality MRI-photoacoustic-Raman nanoparticle. Nat Med. 2012;18(5):829–834.
10. Kim J, Kim HS, Lee N, Kim T, Kim H, Yu T, Song IC, Moon WK, Hyeon T. Multifunctional uniform nanoparticles composed of a magnetite nanocrystal core and a mesoporous silica shell for magnetic resonance and fluorescence imaging and for drug delivery. Angew Chem Int Ed Engl. 2008;47(44):8438–8441.
11. Fan W, Shen B, Bu W, Chen F, Zhao K, Zhang S, Zhou L, Peng W, Xiao Q, Xing H, Liu J, Ni D, He Q, Shi J. Rattle-structured multifunctional nanotheranostics for synergetic chemo-/radiotherapy and simultaneous magnetic/luminescent dual-mode imaging. J Am Chem Soc. 2013;135(17):6494–6503.
12. Yang H, Zhuang YM, Sun Y, Dai AT, Shi XY, Wu DM, Li F, Hu H, Yang S. Targeted dual-contrast T_1- and T_2-weighted magnetic resonance imaging of tumors using multifunctional gadolinium-labeled superparamagnetic iron oxide nanoparticles. Biomaterials. 2011;32(20):4584–4593.
13. Li Z, Yi PW, Sun Q, Lei H, Zhao HL, Zhu ZH, Smith SC, Lan MB, Lu GQ (Max). Ultrasmall water-soluble and biocompatible magnetic iron oxide nanoparticles as positive and negative dual contrast agents. Adv Funct Mater. 2012;22(11):2387–2393.
14. Zhou ZJ, Huang DT, Bao JF, Chen QL, Liu G, Chen Z, Chen X, Gao J. A synergistically enhanced T_1-T_2 dual-modal contrast agent. Adv Mater. 2012;24(46):6223–6228.
15. Choi JS, Lee JH, Shin TH, Song HT, Kim EY, Cheon J. Self-confirming "AND" logic nanoparticles for fault-free MRI. J Am Chem Soc. 2010;132(32):11015–11017.

16. Shin TH, Choi JS, Yun S, Kim IS, Song HT, Kim Y, Park KI, Cheon J. T_1 and T_2 dual-mode MRI contrast agent for enhancing accuracy by engineered nanomaterials. ACS Nano. 2014;8(4):3393–3401.
17. Della Rocca J, Liu D, Lin W. Nanoscale metal-organic frameworks for biomedical imaging and drug delivery. Acc Chem Res. 2011;44(10):957–968.
18. Alley MC, Scudiero DA, Monks A, Hursey ML, Czerwinski MJ, Fine DL, Abbott BJ, Mayo JG, Shoemaker RH, Boyd MR. Feasibility of drug screening with panels of human tumor cell lines using a microculture tetrazolium assay. Cancer Res. 1988;48(3):589–601.
19. Lee HJ, Park JU, Choi S, Son J, OH M. Synthesis and photoluminescence properties of Eu3+-doped silica@coordination polymer core-shell structures and their calcinated silica@Gd2O3:Eu and hollow Gd2O3: Eu microsphere products. Small. 2013;9(4):561–569.
20. Kuda-Wedagedara ANW, Wang CC, Martin PD, Allen MJ. Aqueous Eu-II-containing complex with bright yellow luminescence. J Am Chem Soc. 2015; 137(15):4960–4963.
21. Liz-Marzan LM, Giersig M, Mulvaney P. Synthesis of nanosized gold-silica core-shell particles. Langmuir. 1996;12(18):4329–4335.
22. Chen H, Wang GD, Chuang YJ, Zhen Z, Chen X, Biddinger P, Hao Z, Liu F, Shen B, Pan Z, Xie J. Nanoscintillator-mediated X-ray inducible photodynamic therapy for in vivo cancer treatment. Nano Lett. 2015;15(4):2249–2256.
23. Luo YX, Zhang JF, Sun AH, Chu CY, Zhou S, Guo JJ, Chen T, Xu G. Electric field induced structural color changes of SiO2@TiO2 core-shell colloidal suspensions. J Mater Chem C Mater Opt Electron Devices. 2014;2(11):1990–1994.
24. Kang JG, Jung Y, Min BK, Sohn Y. Full characterization of Eu(OH)(3) and Eu2O3 nanorods. Appl Surf Sci. 2014;314:158–165.
25. Peng MY, Hong GY. Reduction from Eu3+ to Eu2+ in BaAl2O4:Eu phosphor prepared in an oxidizing atmosphere and luminescent properties of BaAl2O4:Eu. J Lumin. 2007;127(2):735–740.
26. Wang Z, Li P, Guo Q, Yang Z. Solid-state synthesis and luminescent properties of yellow-emitting phosphor NaY(MoO4)2:Dy3+ for white light-emitting diodes. Luminescence. 2015;30(6):842–846.
27. Cowger TA, Tang W, Zhen Z, Hu K, Rink DE, Todd TJ, Wang GD, Zhang W, Chen H, Xie J. Casein-coated Fe5C2 nanoparticles with superior r2 relaxivity for liver-specific magnetic resonance imaging. Theranostics. 2015;5(11):1225–1232.
28. Wartenberg N, Fries P, Raccurt O, Guillermo A, Imbert D, Mazzanti M. A gadolinium complex confined in silica nanoparticles as a highly efficient T_1/T_2 MRI contrast agent. Chemistry. 2013;19(22):6980–6983.
29. Estelrich J, Sanchez-Martin MJ, Busquets MA. Nanoparticles in magnetic resonance imaging: from simple to dual contrast agents. Int J Nanomedicine. 2015; 10:1727–1741.
30. Ruoslahti E. RGD and other recognition sequences for integrins. Annu Rev Cell Dev Biol. 1996;12:697–715.
31. Cai W, Chen X. Multimodality molecular imaging of tumor angiogenesis. J Nucl Med. 2008;49(*Suppl* 2):113S–128S.
32. Moghimi SM, Hunter AC, Murray JC. Long-circulating and target-specific nanoparticles: Theory to practice. Pharmacol Rev. 2001;53(2):283–318.
33. Canet E, Douek P, Janier M, Bendid K, Amaya J, Millet P, Janier M. Influence of bolus volume and dose of gadolinium chelate for first-pass myocardial perfusion MR imaging Studies. J Magn Reson Imaging. 1995;5(4):411–415.
34. Kostler H, Ritter C, Lipp M, Beer M, Hahn D, Sandstede J. Prebolus quantitative MR heart perfusion Imaging. Magn Reson Med. 2004;52(2):296–299.